Sensor Fusion for Improved Control of Piezoelectric Tube Scanners

Andrew J. Fleming* Adrian Wills* S. O. Reza Moheimani*
*School of Electical Engineering and Computer Science, The University of Newcastle, NSW, Australia

***Abstract*— In this work the measurement quality of capacitive displacement sensors is augmented with the high dynamic sensitivity of piezoelectric transducers. By combining the low-frequency performance and stability of capacitive sensors with the high sensitivity and bandwidth of piezoelectric transducers, a displacement RMS noise of 1 nm and range of 100 μm is achieved with a bandwidth of 20 kHz. The composite displacement signal is employed with a receding horizon control strategy to achieve high-speed low-noise control of a piezoelectric tube scanner.**

***Index Terms*— Sensor fusion, capacitive sensor, piezoelectric strain sensor, tube scanner**

I. Introduction

A piezoelectric tube scanner is a thin cylinder of radially poled piezoelectric material, fixed at the base and free to vibrate elsewhere, with four external electrodes and a grounded internal electrode. Figure 1 shows a tube scanner developing a lateral tip deflection in response to an applied voltage. When a voltage is applied to one of the external electrodes, the actuator wall expands, and due to Poisson coupling, causes a vertical contraction and large lateral deflection of the tube tip.

Piezoelectric tubes are used extensively in applications requiring precision positioning such as Scanning Probe Microscopy [2]–[4], [14], nanofabrication systems [10], [20] and nanomanipulation devices [15], [21]. In these applications, piezoelectric tubes are designed with large length to diameter ratios, this provides a large lateral deflection range but imposes low mechanical resonance frequencies. In nanometer precision raster scanning applications, such as scanning probe microscopy, the maximum triangular scan rate is limited to around 1-10 % of the first resonance frequency. To illustrate the problem, consider a typical piezoelectric tube with maximum lateral deflection of 100 μm and a resonance frequency of 700 Hz. For a scanning probe microscope, this equates to more than one minute of image acquisition time (at 640×480 resolution) and severe throughput limitations in nanomanipulation and fabrication processes.

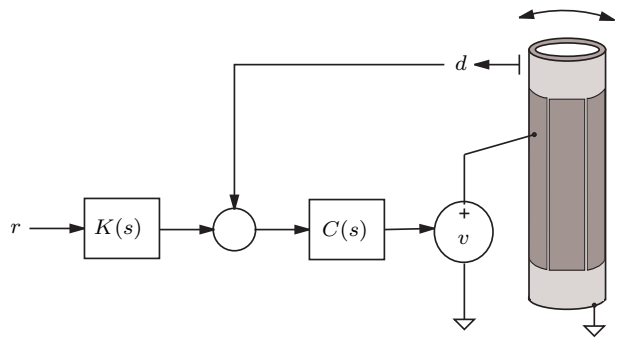

Fig. 1. Voltage driven tube scanner with reference input r, feedforward filter $K(s)$, displacement measurement d, and feedback controller $C(s)$

Nonlinearity is another on-going difficulty associated with piezoelectric tube scanners (and piezoelectric actuators in general). When employed in an actuating role, piezoelectric transducers display a significant hysteresis in the transfer function from an applied voltage to strain or displacement [1]. Due to hysteresis, ideal scanning signals can result in severely distorted tip displacements, and hence poor image quality and poor repeatability in nanofabrication processes.

Techniques aimed at addressing both mechanical dynamics and hysteresis can be grouped generally into two broad categories: feedforward, for example [6], [7], [12], [17]; and feedback, for example [16], [19]. Feedback control of piezoelectric tube scanners and nano-positioners is generally accomplished with the aid of a capacitive, inductive, or optical displacement sensor. With the exception of interferometers which are prohibitively expensive for commercial applications, and if the target can be adequately grounded, capacitive sensors offer the greatest resolution and signal-to-noise ratio. Again with the exception of interferometers, all of the techniques mentioned are severely limited in bandwidth if high resolutions or dynamic ranges are required. As an example, consider a typical commercial grade capacitive sensor with a range of ± 5 μm and an RMS noise of $1\text{nm}/\sqrt{\text{Hz}}$. To achieve an RMS noise of 10 nm, i.e., a signal-to-noise ratio of 50 dB (at full scale), the bandwidth must be limited to 100 Hz.

In this work we demonstrate the combination of capacitive sensing and piezoelectric strain voltage measurement for high performance displacement estimation. By combining the low-frequency performance and stability of capacitive sensors with the high sensitivity and bandwidth of piezoelectric transducers, we demonstrate a signal-to-noise ratio of 90 dB (bipolar 16 bit) at a full-scale range of ± 100 μm and bandwidth of 20 kHz. These ideas are applicable to transducers such as piezoelectric tubes and kinematic positioning stages with integrated piezoelectric strain sensors.

With the aid of a low-variance displacement and state estimation it is possible to construct either an output- or state-feedback control system. In this work, receeding horizon control is selected for its ease-of-implementation and its suitable objective function which is equivalent to minimizing tracking error over a finite horizon.

This paper proceeds with a description of the scanner

1-4244-1264-1/07/$25.00 ©2007 IEEE

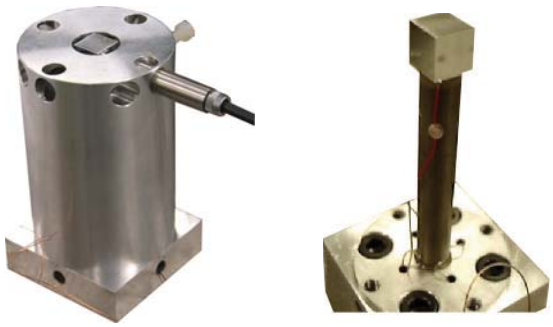

(a) (b)

Fig. 2. The piezoelectric tube mounted inside an aluminium shield. The x-axis capacitive sensor is shown secured at right angles to a cube mounted onto the tube tip

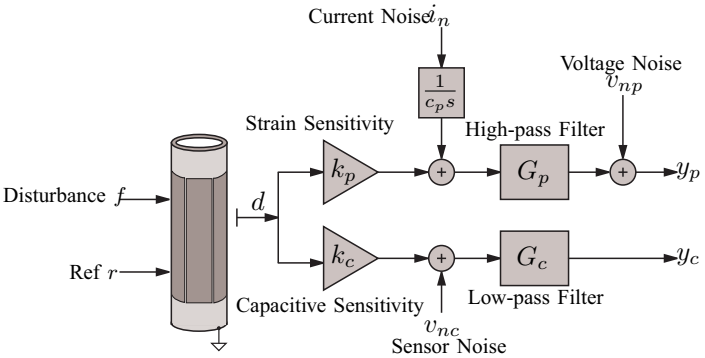

Fig. 3. The signal path and additive noise from the applied voltage to the measured strain voltage and capacitive sensor output.

apparatus in Section II, then a discussion of signal properties and displacement estimation in Section III. Receding horizon control is introduced in Section IV followed by experimental results in Section V.

II. Scanning Apparatus

As pictured in Figure 2, the apparatus used in this work comprises a piezoelectric tube housed in a removable aluminium shield. A polished, hollow aluminium cube 8 mm square (1.5 g in mass) is glued to the tube tip to allow displacement measurements with an ADE Tech 4810 Gauging Module and 2804 capacitive sensor. The sensitivity of the capacitive sensor is 100 mV/μm over a range of $\pm$100 μm and bandwidth of 10 kHz. During assembly, the shield serves as a jig to ensure the tube is both vertical and alligned in the same axis as the cube face and capacitive sensor head. Nylon grub screws secure the sensor heads after assembly.

The tube was manufactured by Boston PiezoOptics from high-density PZT-5H piezoceramic. Physical dimensions can be found in reference [9]. The electrodes are driven with an in-house $\pm 200V$ charge amplifier [9]. Charge amplifiers have been shown to reduce hysteresis in piezoelectric tube scanners by 89%, see [8] and [9] for details.

The tip displacement frequency response, measured using an HP 35670A spectrum analyzer, is plotted in Figure 5. The free response has a first resonance at 850 Hz and a static sensitivity of 171 nm per volt. To evaluate performance robustness in the following sections, a worst case mass of 1.5 g is affixed to the top cube surface. The additional mass reduces the resonance frequency by 110 Hz or 13%.

III. Sensor Design

A. Signal Characteristics

The available displacement signals: capacitive, piezoelectric, and simulated; are illustrated in Figure 3. The characteristics and statistical properties of each signal are discussed in the following.

Simulated Displacement $y_m(s) = r(s)G(s)$. The simulated displacement is the result of filtering the measured input r with a dynamic model of the scanner dynamics G. Controlling the simulated output y_m is equivalent to performing model-based feedforward control. The output y_m is subject to large uncertainties due to model mismatch, temperature variation and load changes. The sensitivity of $G(s)$ should be periodically calibrated using the capacitive sensor.

Capacitive Sensor y_c. A capacitive sensor applies a high-frequency potential between two plates, the resulting current is proportional to capacitance and displacement. The displacement sensitivity is highly stable and largely invariant to temperature and environmental conditions; it is the most reliable measurement.

As shown in Figure 3, the displacement signal is the filtered sum of the true displacement d and additive white noise v_{nc}. As discussed in the introduction, a low-pass filter G_c provides an arbitrary resolution at the expense of bandwidth. The capacitive sensor provides an accurate method for callibration of the simulated model and strain measurement. Capacitive sensors are also excellent for recording system frequency responses, for example, the transfer function from an applied voltage to displacement. Multi-cycle swept-sine and averaged periodically excited FFT measurements are two statistically consistent methods for procuring system frequency response functions.

Piezoelectric Strain Voltage y_p. The piezoelectric strain voltage v_p is proportional to the strain ε and tip displacement d below the resonance frequency. The constant k_ε, relating the piezoelectric strain voltage to tip deflection, is a function of the scanner geometry, material properties, and piezoelectric strain constant.

Due to the high source impedance, especially at low frequencies, care must be taken to avoid contamination by interference and loss due to parasitic capacitance and leakage. An acceptable solution is triaxial cable with the outer sheath grounded at the instrument case and connected to one terminal of the transducer. The inner conductor is connected to the transducers high-impedance terminal with an intermediate shield driven by a buffer stage to eliminate parasitic capacitance and leakage. The buffer should be a high transconductance FET or MOSFET common drain amplifier or FET input op amp.

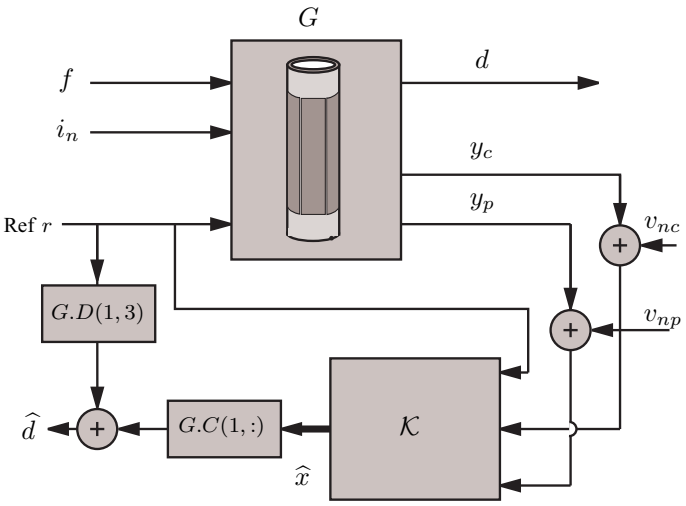

Fig. 4. A Kalman displacement estimator $\mathcal{K}$. The displacement output matrix $C(1,:)$ and feedthrough $D(1,3)$ yield the estimated displacement $\widehat{d}$ from the optimal state estimation $\widehat{x}$. f and i_n are the disturbance force and measurement noise-current, while d, y_c, and y_p are the actual deflection, the capacitive sensor measurement, and the strain voltage measurement.

The transducer capacitance c_p together with the lumped dielectric leakage and external resistance r_p creates the first-order high-pass filter

$$G_p(s) = \frac{s}{s + \frac{1}{r_p c_p}}. \tag{1}$$

The dominant noise processes v_{np} and i_n are the input voltage noise and current noise of the buffer stage respectively. Due to the high source impedance at frequencies below 1 kHz, buffer current noise is of the greatest concern. Although the true current noise filter is a leaky integrator $\frac{1}{c_p s + 1/r_p}$ with breakpoint $\omega = \frac{1}{r_p c_p}$, it is approximated as a pure integrator $\frac{1}{c_p s}$ as shown in Figure 3. The justification for this simplification is in the nature of the current noise density. Both the voltage and current noise density increase at lower frequencies with a first-order break-point of around 1 to 100 Hz. The low frequency increase in current noise density approximately cancels the integrator leakage yielding a white current noise density and pure integrator. Voltage noise is insignificant by comparison at low frequencies.

B. Kalman Sensor Fusion

An automated choice of estimator is a linear observer or Kalman filter [5]. With the assumption of Gaussian distributed random disturbance and measurement noise, a Kalman filter provides the minimum variance state estimate.

Figure 4 illustrates the physical system (Figure 3) 'repackaged' as a system block diagram. The noise input v_{nc} has been approximated as pure measurement noise, this simplifies the design process with negligible error. The discretized system G described below incorporates all of the mechanical and electrical dynamics including noise filters, sensor dynamics, and amplifier dynamics.

$$\begin{aligned} x_{t+1} &= \mathbf{A}x_t + \mathbf{B}\begin{bmatrix} f \\ i_n \\ r \end{bmatrix} \\ \begin{bmatrix} d \\ y_c \\ y_p \end{bmatrix} &= \mathbf{C}x_t + \mathbf{D}\begin{bmatrix} f \\ i_n \\ r \end{bmatrix} \end{aligned} \tag{2}$$

where A, B, C and D are the system matrices of G procured, for example, by system identification or manipulation of the individual transfer functions. The Matlab function `connect` is useful for this purpose.

Based on the variance of the disturbance $\mathbf{Q}$ and measurement noise $\mathbf{R}$, defined as

$$\begin{aligned} \mathbf{Q} &= E\left\{ \begin{bmatrix} f \\ i_n \end{bmatrix} \begin{bmatrix} f & i_n \end{bmatrix} \right\} \\ \mathbf{R} &= E\left\{ \begin{bmatrix} v_{nc} \\ v_{np} \end{bmatrix} \begin{bmatrix} v_{nc} & v_{np} \end{bmatrix} \right\}, \end{aligned} \tag{3}$$

a Kalman observer that minimizes

$$J = \lim_{t\to\infty} E\left\{ [x_t - \widehat{x_t}]\,[x_t - \widehat{x_t}]' \right\} \tag{4}$$

can be found through the solution of an algebraic Ricatti equation [18]. The magnitude of $\mathbf{Q}$ and $\mathbf{R}$ expresses the relative confidence in the measured variables and defines the frequency regions where each signal is dominant. Note, as the noise i_n is integrated, the Kalman filter will always have zero sensitivity to constant error in the measured piezoelectric strain voltage, a desirable property.

C. Estimator Variance Improvement

In many applications the frequency dependent nature of the capacitive and strain signals can be exploited to significantly improve the displacement estimate. One particular method can be used in cases where the desired scan trajectory consists of a large low-frequency component and smaller high-frequency components, for example, a scanning probe microscope triangular scanning pattern.

In a 100 μm, 10 Hz triangular scan, the majority of signal power lies in the first few harmonics. The input impedance of the piezoelectric strain voltage buffer can be dropped to a few hundred kΩs in order to increase the high-pass cut-off frequency to 100 Hz. Now the majority of low-frequency signal power, that would usually comprise 90% of the signal amplitude, has been reduced by 20 dB. This allows the strain voltage gain to be increased by a factor of 10 without worry of saturation, which affords an increase in dynamic range by 20 dB. The combination of low measurement noise associated with the piezoelectric strain voltage, and low-bandwidth of the capacitive sensor provides a displacement sensing technique with dynamic range and signal-to-noise ratio exceeding 16 bit or 90 dB.

The obvious disadvantage of this approach is that dynamic range is only improved so long as the fundamental frequency of the scan signal does not enter the bandwidth of the strain voltage measurement. If it were to, the size of the scan signal would be limited to one tenth its full scale range to avoid saturation.

IV. Receding Horizon Control

The purpose of fusing the signals y_p and y_c is to obtain an estimate of the tube displacement $\hat{d}$ over a wide bandwidth. With such an estimate, a controller is designed in this section using the receding horizon framework. The major benefits of receding horizon control are: 1) it is inherently discrete and straight-forward to implement in real-time; 2) only places a penalty on tracking error over a finite horizon time not infinity as in LQG; and 3) it allows simultaneous design of feedforward and feedback controllers.

Alternative controllers include almost any state- or output-feedback controller (based on $\hat{d}$). One simple controller that was also tested is a Positive Position Feedback controller [11] with FIR feedforward compensation.

A receding horizon control strategy results in the control law:

$$u_t = K\bar{x}_t, \tag{5}$$

The receding horizon framework minimizes a cost function J in order to obtain the next control action u_{t+1}. Then at the next time interval, based on new measurements, the process is repeated again but this time generating u_{t+2}. While the cost function J can be quite general, for the purposes of this application we consider

$$\begin{array}{l} J(u_{t+1|t},\ldots,u_{t+N|t}) \triangleq \\ \frac{1}{2}\sum_{k=1}^{N} ||\widehat{y}_{t+k|t} - r_{t+k}||_Q^2 + ||u_{t+k|t} - u_{t+k-1|t}||_S^2. \end{array} \tag{6}$$

In the above, $\hat{y}_{t+k|t}$ is a prediction of the system output at some future time $t+k$ based on measurements up to and including the current time t. The quadratic form $||\hat{y}_{t+k|t} - r_{t+k}||_Q^2 \triangleq (\hat{y}_{t+k|t} - r_{t+k})^T Q(\hat{y}_{t+k|t} - r_{t+k})$ is included to penalize deviations of the predicted output from future reference values r_{t+k}. Furthermore, the notation $u_{t+k|t}$ is used to highlight that these are future inputs based on information up to and including time t and $||u_{t+k|t} - u_{t+k-1|t}||_S^2$ is included to penalize control movements.

Hence, at time t we can compute the optimal sequence of control movements $\left\{u^\star_{t+1|t},\ldots,u^\star_{t+N|t}\right\}$ via

$$\begin{array}{l} \left\{u^\star_{t+1|t},\ldots,u^\star_{t+N|t}\right\} = \\ \arg\min_{u_{t+1|t},\ldots,u_{t+N|t}} J(u_{t+1|t},\ldots,u_{t+N|t}), \end{array} \tag{7}$$

and then apply $u^\star_{t+1|t}$ at the next time interval $t+1$.

In order to compute $u^\star_{t+1|t}$, we need to be able to predict the output y_{t+k} for $k = 1,\ldots,N$. To achieve this, we employ a state-space model and Kalman filter as discussed in section III-B. Due to page limitations, the remaining standard derivation of receding horizon control is omitted, but can be found in reference [22], or obtained by emailing the first author.

V. Experimental Results

Results are presented in the following that demonstrate the efficacy of sensor fusion and receding horizon control in dynamic positioning applications. As discussed in Section II, we consider two cases, one where the scanner is operated under nominal conditions, and another where a significant load is affixed to the tip.

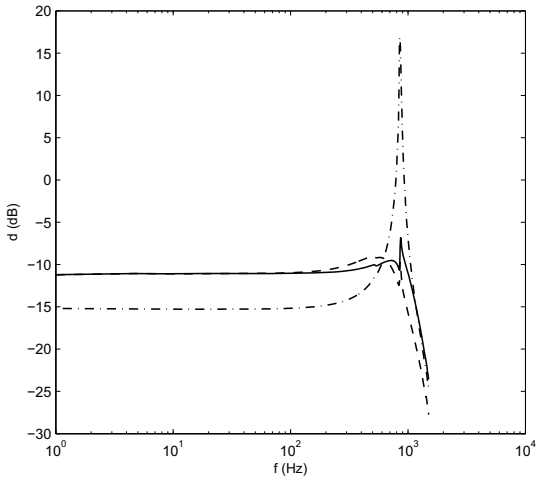

Fig. 5. The open- and closed-loop scanner frequency response measured from the reference input to the tip displacement (in μm/V); open-loop ($\cdots$), unloaded (—), with 1.5 g compliant mass (- -).

In order to procure a model of the system G (Figure 4) the frequency response functions from r to all outputs were acquired with an HP 35670A spectrum analyzer. The displacement d was measured using a Polytec PI PSV300 laser vibrometer

The dynamics of G were obtained using a frequency domain system identification algorithm [13] [1]. The disturbance input f was chosen equivalent to r, and the dynamics due to i_n set as an integrator. The concatenated plant including disturbance inputs f and i_n, the reference input r, the measured and reference outputs y_c, y_p and d, and the performance output z, was assembled using the Matlab function `connect`. As the control system is implemented digitally, a single delay is added to the reference input to account for conversion and processing delay.

The Matlab function `kalman` was used to design the Kalman estimator $\mathcal{K}$. Due to the syntax of `kalman`, a new system is required with outputs y_c and y_p, and inputs reversed, i.e. r is the first input, followed by f and i_n. With $Q = \mathbf{I}$, and

$$R = \alpha \begin{bmatrix} 1 & 0 \\ 0 & E\{i_n\} \end{bmatrix} \tag{8}$$

the parameters α and $E\{i_n\}$ can be varied to express confidence in the measured variables and manipulate the frequency regions where y_c and y_p are dominant.

In order to compute the controller gain matrix K in Section IV, we need to specify the parameters N, Q, S. In this experiment $N = 200$, $Q = 0.1$ and $S = 0.2$.

The estimator and controller were implemented using the Real Time Workshop for Matlab and a dSpace DS1103 DSP prototyping system. The open- and closed-loop frequency responses, plotted in Figure 5, show a peak reduction of at least 24 dB in both the nominal and perturbed response.

[1] An implementation of the multivariable frequency domain subspace algorithm by McKelvey et. al. [13] is available by contacting the first author.

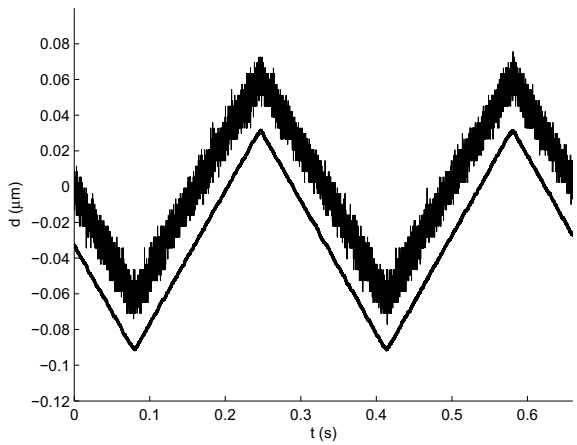

Fig. 6. A 3 Hz 120 nm closed-loop scan; capacitive sensor (top), estimator (bottom).

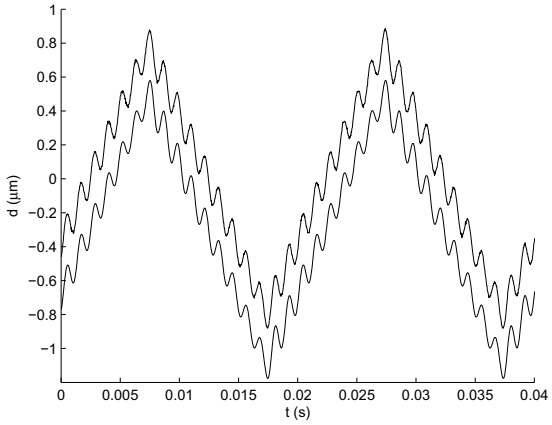

Fig. 7. A 50 Hz 1.6 μm open-loop scan; capacitive sensor (top), estimator (bottom).

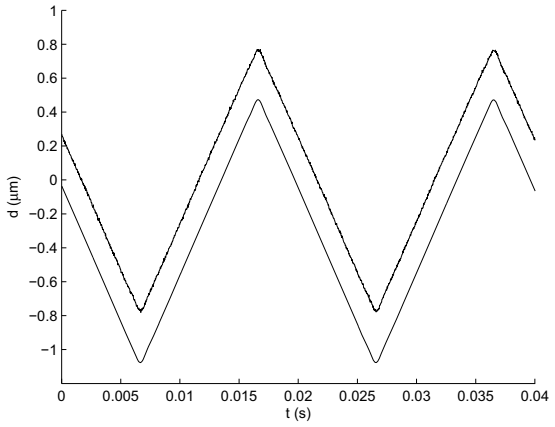

Fig. 8. A 50 Hz 1.6 μm closed-loop scan; capacitive sensor (top), estimator (bottom).

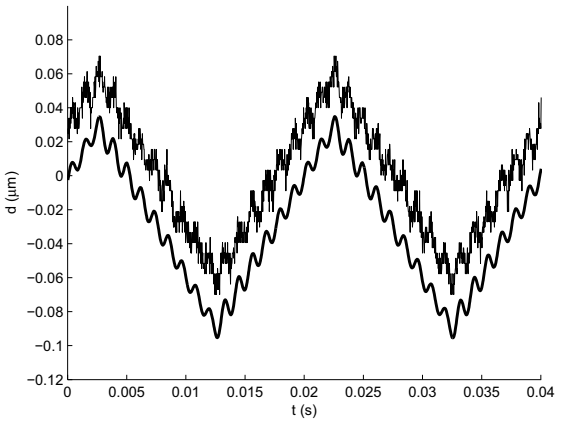

Fig. 9. A 50 Hz 120 nm open-loop scan; capacitive sensor (top), estimator (bottom).

To evaluate the noise and dynamic performance in the time domain, we must consider a number of scenarios. A series of experiments are described below that evaluate the large-signal static and dynamic displacement accuracy, noise-performance, and dynamic performance.

Low Frequency, Small Amplitude (Figure 6). In this experiment the scan amplitude is 120 nm, or 0.06 % of the capacitive sensor range. The capacitive sensor is approaching the limit of its dynamic range (16 bit, or 90 dB) and displays a significant noise component. In contrast, the estimated displacement shows no sign of quantization error and has an unfiltered RMS noise of approximately 1 nm (sampled at 40 kHz). The dynamic range, or the ratio of the largest to smallest signal that can be resolved at full bandwidth is approximately 100 dB. These figures are approximate (but conservative) as it is impossible to differentiate the measurement noise from mechanical disturbance.

High Frequency, High Amplitude (Open-loop Figure 7, closed-loop Figure 8). In Figure 7, a 50 Hz 1.6 μm scan is chosen that clearly excites the mechanical resonance with its 17th harmonic. Although this is a worst case scenario, it clearly illustrates the errors that usually occur on a smaller scale. A simple feedforward controller would effectively reduce this error by nine tenths or more without significantly distorting the scanning signal. In this experiment, where sensor noise is not significant, the controller successfully attenuates resonant dynamics by 24 dB.

High Frequency, Low Amplitude (Open-loop Figure 9, closed-loop Figure 10). In this experiment the control performance is examined at low amplitudes. It is clear from Figures 9 and 10 that the controller works effectively to reduce vibration even at low amplitudes. The excellent noise performance of the state estimate affords a high gain controller without significantly increasing measurement-noise-induced displacement error.

Performance Robustness As can be ascertained from the nominal and perturbed closed-loop frequency response ,

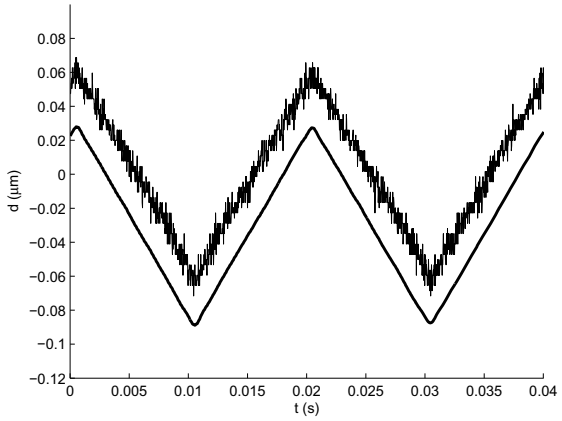

Fig. 10. A 50 Hz 120 nm closed-loop scan; capacitive sensor (top), estimator (bottom).

Figure 5, the tip mass has little effect on the estimate quality and control performance. Triangular scanning accuracy was slightly reduced around the turning points but the degredation in the linear region was negligible.

VI. Conclusions

In addition to capacitive or inductive sensors, a piezoelectric strain sensor can provide large increases in measurement performance at little cost. A piezoelectric tube scanner is a special case where a redundant electrode can provide high precision sensing. The only significant cost is the reduction in displacement range that could be achieved with a second voltage amplifier driving the electrode used for sensing.

Although high sensitivity piezoelectric materials, such as PZT-5H, exhibit significant temperature dependence and poor signal qualities at low-frequencies, a technique is presented here to utilize only the desirable characteristics of each sensor collaboratively. With a model of the sensor dynamics and a linear estimator or Kalman filter, significant improvements to noise performance and dynamic range can be realized.

Experiments on a standard piezoelectric tube, as utilized in scanning probe microscopes, demonstrate an RMS displacement noise of 1 nm (sampled at 40 kHz) with a full-scale range of ± 100 μm. The estimation technique lends itself easily to the inclusion of high-performance state-dependent controllers. A receding horizon control strategy was implemented and proven to attenuate resonant mechanical dynamics by 24 dB without increasing displacement noise (within the limits of measurement). Both the controller and Kalman estimator were insensitive to the dominant uncertainty - large variations in the resonance frequency.

Present and future work includes extending the technique to other nanopositioning applications where high dynamic range, low-noise and wide-bandwidth displacement feedback is required. Examples include kinematic stages with multiple axis and systems with different transducer arrangements, e.g., electromagnetically driven stages with strain and velocity feedback.

Acknowledgments

This work was supported by the Australian Research Council and the Center for Complex Dynamic Systems and Control.

References

[1] H. J. M. T. A. Adriaens, W. L. de Koning, and R. Banning, "Modeling piezoelectric actuators," *IEEE/ASME transactions on mechatronics*, vol. 5, no. 4, pp. 331–341, December 2000.

[2] B. Bhushan, Ed., *The handbook of nanotechnology*. Springe-Verlag, 2004.

[3] G. Binnig and D. P. E. Smith, "Single-tube three-dimensional scanner for scanning tunneling microscopy," *Review of Scientific Instruments*, vol. 57, no. 8, pp. 1688–1689, August 1986.

[4] D. A. Bonnell, Ed., *Scanning Probe Microscopy and Spectroscopy - Theory, Techniques and Applications. Second Edition*. John Wiley & Sons, 2001.

[5] R. G. Brown and P. Hwang, *Introduction to Random Signals and Applied Kalman Filtering*. John Wiley and Sons Inc., 1997.

[6] D. Croft, D. McAllister, and S. Devasia, "High-speed scanning of piezo-probes for nano-fabrication," *Transactions of the ASME, Journal of Manufacturing Science and Technology*, vol. 120, pp. 617–622, August 1998.

[7] D. Croft, S. Stilson, and S. Devasia, "Optimal tracking of piezo-based nanopositioners," *Nanotechnology*, vol. 10, pp. 201–208, 1999.

[8] A. J. Fleming and S. O. R. Moheimani, "A grounded load charge amplifier for reducing hysteresis in piezoelectric tube scanners," *Review of Scientific Instruments*, vol. 76, no. 7, July 2005. [Online]. Available: PDFs/J05d.pdf

[9] ——, "Sensorless vibration suppression and scan compensation for piezoelectric tube nanopositioners," *IEEE Transactions on Control Systems Technology*, vol. 14, no. 1, pp. 33–44, January 2006. [Online]. Available: PDFs/J06b.pdf

[10] B. D. Gates, Q. Xu, J. C. Love, D. B. Wolfe, and G. M. Whitesides, "Unconventional nanofabrication," *Annual Reviews of Materials Research*, vol. 34, p. 339372, 2004.

[11] J. L. Fanson and T. K. Caughey, "Positive Position Feedback Control for Large Space Structures," *AIAA Journal*, vol. 28, no. 4, pp. 717–724, 1990.

[12] K. Leang and S. Devasia, "Iterative feedforward compensation of hysteresis in piezo positioners," in *Proc. IEEE Conference on Decision and Control*, Maui, HI, December 2003.

[13] T. McKelvey, H. Akcay, and L. Ljung, "Subspace based multivariable system identification from frequency response data," *IEEE Transactions on Automatic Control*, vol. 41, no. 7, pp. 960–978, July 1996.

[14] E. Meyer, H. J. Hug, and R. Bennewitz, *Scanning Probe Microscopy*. Heidelberg, Germany: Springer, 2004.

[15] F. J. Rubio-Sierra, W. M. Heckle, and R. . W. Stark, "Nanomanipulation by atomic force microscopy," *Advanced Engineering Materials*, vol. 7, no. 4, pp. 193–196, 2005.

[16] S. Salapaka, A. Sebastian, J. P. Cleveland, and M. V. Salapaka, "High bandwidth nano-positioner: A robust control approach," *Review of Scientific Instruments*, vol. 75, no. 9, pp. 3232–3241, September 2002.

[17] G. Schitter, R. W. Stark, and A. Stemmer, "Fast contact-mode atomic force microscopy on biological specimens by model-based control," *Ultramicroscopy*, vol. 100, pp. 253–257, 2004.

[18] S. Skogestad and I. Postlethwaite, *Multivariable Feedback Control*. John Wiley and Sons, 1996.

[19] N. Tamer and M. Dahleh, "Feedback control of piezoelectric tube scanners," in *Proc. American Control Conference*, Lake Buena Vista, FL, December 1994, pp. 1826–1831.

[20] A. A. Tsenga, A. Notargiacomob, and T. P. Chen, "Nanofabrication by scanning probe microscope lithography: A review," *Journal of Vacuum Science and Technology*, vol. 23, no. 3, pp. 877–894, May/June 2005.

[21] W. Vogl, B. Kai-Lam Ma, and M. Sitti, "Augmented reality user interface for an atomic force microscope-based nanorobotic system," *IEEE Transactions on Nanotechnology*, vol. 5, no. 4, pp. 397–406, July 2006.

[22] A. Wills, "EE04025 notes on linear model predictive control," Electrical Engineering, University of Newcastle, Tech. Rep., 2004.